EOS

Monitoring Earth Surface Dynamics With Optical Imagery

PAGES 1–2

The increasing availability of high-quality optical satellite images should allow, in principle, continuous monitoring of Earth's surface changes due to geologic processes, climate change, or anthropic activity. For instance, sequential optical images have been used to measure displacements at Earth's surface due to coseismic ground deformation [e.g., *Van Puymbroeck et al.*, 2000], ice flow [*Scambos et al.*, 1992; *Berthier et al.*, 2005], sand dune migration [*Crippen*, 1992], and landslides [*Kääb*, 2002; *Delacourt et al.*, 2004].

Surface changes related to agriculture, deforestation, urbanization, and erosion—which do not involve ground displacement—might also be monitored, provided that the images can be registered with sufficient accuracy. Although the approach is simple in principle, its use is still limited, mainly because of geometric distortion of the images induced by the imaging system, biased correlation techniques, and implementation difficulties.

These obstacles have been overcome thanks to recent methodological advances and the development of a user-friendly software package called Co-Registration of Optically Sensed Images and Correlation (COSI-Corr) [*Leprince et al.*, 2007]. The software makes it possible to coregister images and to measure surface displacements with unprecedented ease and accuracy. This article describes some applications of the technique and pinpoints some key thematic questions that can benefit from this approach.

Increase of Data Set Availability

The application of the technique depends primarily on the availability of high-quality optical images, for which there exist considerable archived data to mine. Aerial surveys by the U.S. Geological Survey have covered the United States since the 1950s,

By S. Leprince, E. Berthier, F. Ayoub,
C. Delacourt, and J.-P. Avouac

the Institut Géographique National has surveyed the French territory since the 1940s, and similar archives exist across the world. Multiple satellite programs have delivered worldwide coverage such as Landsat since 1972, SPOT since 1986, and the Advanced Spaceborne Thermal Emission and Reflection Radiometer (ASTER) instrument, on board the NASA satellite Terra, since 1999. Many high-resolution satellites have been launched more recently, including IKONOS, QuickBird, OrbView, EROS, and FORMOSAT.

Images acquired by these programs have been essential in assessing temporal changes induced by large-scale natural disasters like earthquakes, tsunamis, floods, and volcanic eruptions. However, precisely quantifying temporal changes between series of images, possibly acquired by different instruments and at different resolutions, remains a considerable challenge.

COSI-Corr Software Package

The COSI-Corr software package allows for automatic and precise orthorectification, coregistration, and subpixel correlation of satellite and aerial images [*Leprince et al.*, 2007]. The procedure does not require external information such as GPS measurements of ground control points, and it is based solely on topographic knowledge and on the ancillary data provided with the observing platform.

In particular, the software package takes advantage of the availability of accurate digital elevation models with global coverage (Shuttle Radar Topography Mission). Subpixel change detection (i.e., correlation) is then applied to the set of orthoimages produced. COSI-Corr makes it possible to measure local displacements between temporal series of images, possibly acquired by different instruments and at different resolutions, with measurement accuracy of the order of a small fraction of the nominal images' resolution.

A plug-in for Environment for Visualizing Images (ENVI) remote sensing software, COSI-Corr is freely available from the California Institute of Technology's Tectonics Observatory (http://www.tectonics.caltech.edu).

Coseismic Deformation

Coseismic deformation is generally studied through field surveys of surface ruptures or geodetic or interferometric synthetic aperture radar (InSAR) measurements. However, these techniques often fail to provide detailed maps of the near-field surface strain, which may consist of a complex of surface ruptures and cracks within a fault zone of finite width. Consequently, InSAR and field measurements are not efficient approaches to estimating the total slip across a fault zone and its along-strike variability.

The distribution of slip, which is critical to understanding earthquake dynamics and the damaging near-field seismic waves, might be best assessed from correlating optical images. Optical-image correlation has proven to be efficient in mapping fault ruptures and in measuring both the fault-parallel and fault-perpendicular components of coseismic displacements [*Avouac et al.*, 2006]. Several studies indicate success in correlating images from the same sensor and with nearly equal incidence views [e.g., *Van Puymbroeck et al.*, 2000; *Dominguez et al.*, 2003; *Klinger et al.*, 2006].

COSI-Corr now allows the processing of images acquired by different systems and with different incidence views, considerably broadening the technique's potential. Figure 1a shows one component of the coseismic displacement field induced by the 1999 M_w 7.1 Hector Mine earthquake in California, measured by correlating a 10-meter SPOT 4 image with a 15-meter ASTER image. Although the deformation field is not as well resolved as the one measured by correlating two SPOT images with 10-meter resolution [*Leprince et al.*, 2007], the fault trace is effortlessly delineated and the fault slip vectors can be measured from the surface displacement discontinuities. A secondary branch of the rupture that accounts for a right lateral displacement of about 1 meter is also visible. This example also demonstrates the subpixel capabilities of COSI-Corr. Even with images from different sensors, uncertainties on the fault slip measurements are very low: 0.15 meter to 0.8 meter.

Ice Flow

In the current climatic context, monitoring continental ice and better understanding glacier dynamics are crucial. *Rignot and*

(a)

secondary fault

-3.0   m   +4.0   3 m

NS Offset (m)

4.55 ± 0.15 m

Distance to fault (Km)

A   A'

Main
fault

Horizontal fault slip vectors are
measured from linear least squares
adjustment on each side of the
fault and on each N-S and E-W
component of profiles running
perpendicularly to the fault.
Profiles are stacked over a width
of 2 km. This produces the vector
plot of the displacement at fault,
showing right-lateral strike-slip
motion. Ellipses represent the
95% confidence interval.

(b)

N

Mer de
Glace

Talèfre

Leschaux

A   A'

B   B'

2000 m

26 days horizontal
displacement (m)
0 5 10 15 20 25 30 35 40 45 50 55

(c)

◇ GPS
    measurements

• Raw correlation
    measurements

— 12.5m
    longitudinal
    average

A - A'

B - B'

Distance (km) along North direction

Displacement in meters over 26 days
0 2 4 6 8 10 12 14 16 18 20

(d)

A —— A'
B —— B'

26 days displacement (m)

Transversal distance (meters)
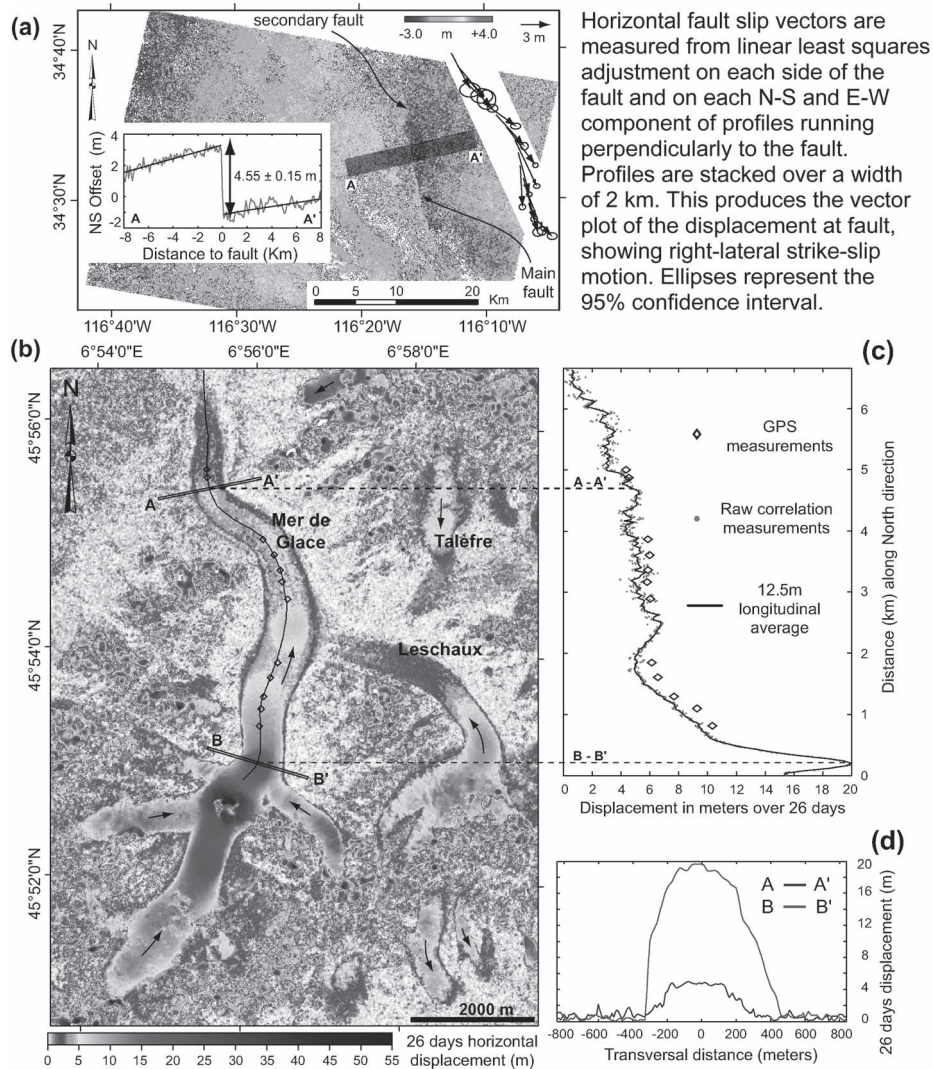-800 -600 -400 -200 0 200 400 600 800

*Fig. 1. (a) North/south component (northward positive) of the coseismic displacement field due
to the 1999 Hector Mine earthquake in California. The pre-earthquake image (10-meter SPOT 4
acquisition from 17 August 1998) and the post-earthquake image (15-meter ASTER acquisi-
tion from 10 May 2000) were orthorectified and coregistered on a 10-meter-resolution grid, and
offsets were measured from subpixel correlation between sliding windows. No measurement is
assigned to white points where the correlation is too weak. The main fault rupture is a linear dis-
continuity in the data. The standard deviation on individual measurements is around 1.3 meters.
(b) Amplitude of the horizontal displacement over the Mer de Glace area from 23 August 2003
to 18 September 2003, obtained from two panchromatic 2.5-meter-resolution SPOT 5 images.
Arrows indicate the flow direction. Displacements below the images' resolution appear in blue.
Displacements as high as 55 meters (about 800 meters per year) are recorded over this 26-day
period. (c) Displacements along a central flow line of the Mer de Glace measured from SPOT 5
images and from campaign GPS. The time period covered by the GPS (12 August 2003 to 3 Sep-
tember 2003) starts slightly earlier in the summer and includes the August 2003 European heat
wave, which explains the faster velocities observed over this period [Berthier et al., 2005].
(d) Displacement along transverse profiles AA' and BB'. Original color image appears at the
back of this volume.*

Kanagaratnam [2006] recently detected that the rapid increase in ice velocities is the major cause of mass reduction of polar ice sheets, but the seasonal and interannual variability of glacier flow remains poorly known. Cross correlation of optical imagery can address these issues [*Kääb*, 2002; *Berthier et al.*, 2005].

Figures 1b, 1c, and 1d show horizontal displacements in the Mer de Glace area (Alps) over 26 days (23 August to 18 September 2003), derived from 2.5-meter-resolution SPOT 5 images. Our study reveals details of the ice velocity field with exceptional accuracy. Very few areas of decorrelation are observed, and when such areas are present, they result mainly from changes in length and orientation of mountain shadows between the two dates. Around the main glaciers, many small, disconnected regions (subkilometric size) have measurable motion. This complete and homogeneous ice flow field measured with COSI-Corr is valuable to validating and calibrating ice flow models, which can then be used to predict the fate of mountain glaciers and ice sheets under global warming scenarios.

"Slow" Landsliding

The mechanics of slowly moving landslides, a common phenomenon in mountainous areas, also remains poorly understood. The dynamics are complex and highly sensitive to climatic factors [*Malet et al.*, 2003], making it difficult to assess how slow landslides evolve with time. Conventional geodetic measurements (tacheometry, leveling, kinematic GPS) are commonly used to monitor the temporal evolution of landslides, but they cannot capture the spatial heterogeneities of mass movement, which may be best assessed with multitemporal images.

Figures 2a and 2b show cumulative horizontal displacement over about 11 months, measured from the subpixel correlation of two 2.5-meter-resolution SPOT 5 images. This displacement field is consistent with InSAR measurements [*Squarzoni et al.*, 2003], but it provides better spatial resolution. Interestingly, the velocity field does not coincide with the geomorphic expression of the landslide and is highly heterogeneous. A network of benchmarks had been installed for repeated geodetic measurements. Although the targets were correctly placed according to the morphology of the landslide, they missed the most active areas. These areas were revealed by our technique and may otherwise have remained undetected.

A Technique Ready for Operational Use

Investigating and monitoring Earth's surface evolution through coregistration and correlation of multitemporal and multisensor images is promising, especially given the existing archives of satellite and aerial images, the increasing number of satellite imagery systems, and their improving resolution. The COSI-Corr methodology corrects pointing inaccuracies in both pushbroom satellites and aerial images to achieve subpixel image coregistration. In addition, the subpixel correlation of precisely coregistered images allows for the accurate estimation of displacement fields between multitemporal images.
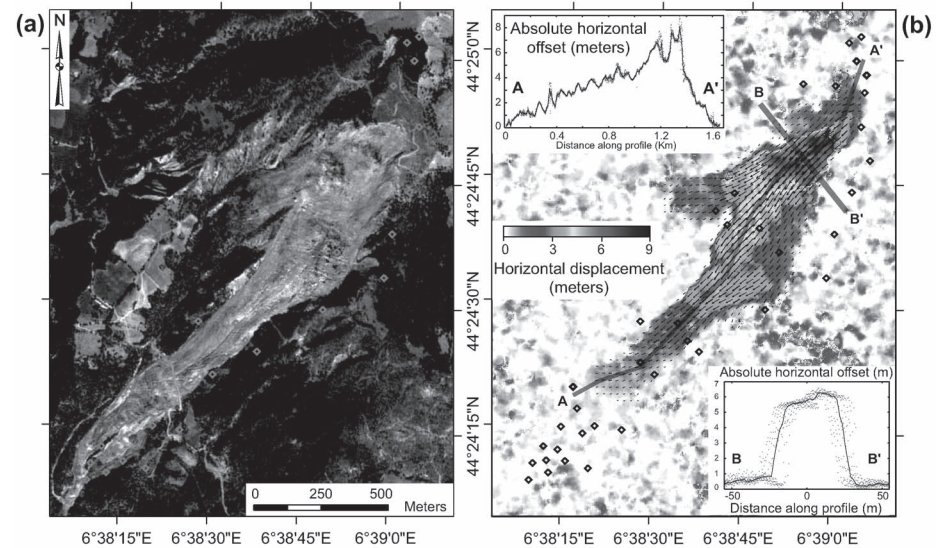

Fig. 2. (a) Orthorectified SPOT image of the La Valette landslide (Ubaye Valley, French Alps). The red diamonds show the geodetic benchmarks for field survey. (b) Absolute horizontal displacement and displacement vectors as imaged from the correlation of two 2.5-meter SPOT 5 images acquired on 19 September 2003 and 22 August 2004. The maximum displacement is 9 meters. Longitudinal and transversal profiles, along AA' and BB', respectively, show the raw data (red dots) and the average over a 15-meter-wide swath (gray line). The black diamonds indicate the geodetic benchmarks. The displacement field revealed from the correlation would not have been noticed in the geodetic measurements. Original color image appears at the back of this volume.

The accuracy of the technique may be limited by the following: availability of accurate digital elevation models, especially in mountainous areas; the quality of ancillary data provided with the images (attitude records should be well sampled); radiometric noise, sensor saturation, and aliasing; shadow length and orientation differences between images; variations in snow, cloud, or vegetation cover; or man-made changes such as new buildings.

Despite these limitations, COSI-Corr is an efficient and versatile tool for investigating a variety of geomorphic and seismotectonic processes such as faulting, the mechanics of ice flow and the effects of climate, and landslides.

This approach has myriad potential applications. For instance, it has also been used to accurately measure sand dune migration. Correlation of optical images is a valuable complement to InSAR for measuring displacements at the Earth's surface because it directly provides the two components of the horizontal displacement field, it is more robust against decorrelation, and it does not saturate if there is a large displacement gradient. Furthermore, because COSI-Corr also allows for accurate coregistration of multispectral bands, applications that require high-quality band-to-band coregistration, such as vegetation monitoring, also can be investigated.

References

Avouac, J. P., F. Ayoub, S. Leprince, O. Konca, and D. V. Helmberger (2006), The 2005, M_w 7.6 Kashmir earthquake: Sub-pixel correlation of ASTER images and seismic waveforms analysis, *Earth Planet. Sci. Lett., 249*(3-4), 514–528.

Berthier, E., H. Vadon, D. Baratoux, Y. Arnaud, C. Vincent, K. L. Feigl, F. Remy, and B. Legresy (2005), Surface motion of mountain glaciers derived from satellite optical imagery, *Remote Sens. Environ., 95,* 14–28.

Crippen, R. E. (1992), Measuring of subresolution terrain displacements using SPOT panchromatic imagery, *Episodes, 15,* 56–62.

Delacourt, C., P. Allemand, B. Casson, and H. Vadon (2004), Velocity field of the "La Clapiere" landslide measured by the correlation of aerial and QuickBird satellite images, *Geophys. Res. Lett., 31,* L15619, doi:10.1029/2004GL020193.

Dominguez, S., J.-P. Avouac, and R. Michel (2003), Horizontal coseismic deformation of the 1999 Chi-Chi earthquake measured from SPOT satellite images: Implications for the seismic cycle along the western foothills of central Taiwan, *J. Geophys. Res., 108*(B2), 2083, doi:10.1029/2001JB000951.

Kääb, A. (2002), Monitoring high-mountain terrain deformation from repeated air- and spaceborne

optical data: Examples using digital aerial imagery and ASTER data, *J. Photogramm. Remote Sens.*, 57(1-2), 39–52.

Klinger, Y., R. Michel, and G. C. P. King (2006), Evidence for an earthquake barrier model from M_w ~ 7.8 Kokoxili (Tibet) earthquake slip-distribution, *Earth Planet. Sci. Lett.*, 242(3-4), 354–364.

Leprince, S., S. Barbot, F. Ayoub, and J. P. Avouac (2007), Automatic, precise, ortho-rectification and co-registration for satellite image correlation: Application to seismotectonics, *IEEE Trans. Geosci. Remote Sens.*, 45, 1529–1558.

Malet, J.-P., A.-V. Auzet, O. Maquaire, B. Ambroise, L. Descroix, M. Estèves, J.-P. Vandervaere, and E. Truchet (2003), Soil surface characteristics influence on infiltration in black marls: Application to the Super-Sauze earthflow (southern Alps, France), *Earth Surf. Processes Landforms*, 28, 547–564.

Rignot, E., and P. Kanagaratnam (2006), Changes in the velocity structure of the Greenland ice sheet, *Science*, 311, 986–990.

Scambos, T. A., M. J. Dutkiewicz, J. C. Wilson, and R. A. Bindschadler (1992), Application of image cross-correlation to the measurement of glacier velocity using satellite image data, *Remote Sens. Environ.*, 42, 177–186.

Squarzoni, C., C. Delacourt, and P. Allemand (2003), Nine years of spatial and temporal evolution of the La Valette landslide observed by SAR interferometry, *Eng. Geol.*, 68, 53–66.

Van Puymbroeck, N., R. Michel, R. Binet, J. P. Avouac, and J. Taboury (2000), Measuring earthquakes from optical satellite images, *Appl. Opt.*, 39, 3486–3494.

Author Information

Sébastien Leprince, Electrical Engineering Department, California Institute of Technology, Pasadena; E-mail: leprincs@caltech.edu; Etienne Berthier, Centre National de la Recherche Scientifique-LEGOS, Toulouse, France; François Ayoub, Geology and Planetary Science Division, California Institute of Technology; Christophe Delacourt, Domaines Océaniques, IUEM, Université de Bretagne Occidentale, Plouzané, France; and Jean-Philippe Avouac, Geology and Planetary Science Division, California Institute of Technology.

The Most Ancient Maps of Erupting Mount Etna

PAGES 2, 5

Mount Etna, in eastern Sicily, Italy, is an active volcano on whose slopes are the city of Catania and several towns. The volcano, whose eruptions are noted in written sources dating back to the thirteenth century B.C., continues to hold surprises for researchers who examine its eruptive history. During extensive historical research for a new catalog of Etna's eruptions (E. Guidoboni and E. Boschi, manuscript in preparation, 2008), two maps have been found that previously were unknown in the literature. These maps, which are the most ancient ones that represent Mount Etna erupting, provide new elements to evaluate the eruption that started on 19 December 1634 and continued until June 1636.

The two maps are important iconographic sources that allow for a more complete picture of that eruption, providing significant and complementary elements to two separate, and also previously unknown, accompanying written reports. In addition, the maps attest to the need during that period of time (shortly after the 1632 publication of Galileo's "Dialogue Concerning the Two Chief World Systems") to describe the ongoing eruptive phenomenon not only in words but also in graphic realistic representation.

The 1634 eruption was only partially known of in the historical catalogues (recalled in 1793 by Ferrara, in 1815 by Recupero, and in 1883 by Mercalli). The eruption is listed in currently used catalogues [*Romano and Sturiale*, 1982; *Tanguy*, 1981; *Siebert and Simkin*, 2002, *Branca and Del Carlo*, 2004] because it was listed in earlier studies, but without any new review of the data or new research.

The two maps, one painted in several colors and the other done just in ink and sepia watercolor, accompany two separate reports by two Jesuits, one Italian and one French, who were eyewitnesses to the phenomenon. The descriptions of the volcano and the ongoing lava flows were made independently by the eyewitnesses, with help from local guides who had an excellent knowledge of the region.

The two large drawings are the most ancient known maps of Etna drawn to depict not just the volcano but an eruption at Mount Etna in progress. Rather than being Mannerist-style drawings or landscape images, they are "scientific" maps that can be used to learn about the 1634 eruption in greater detail.

Map 1: An Apparently Elementary Drawing

Map 1 (Figure 1; 28.8 × 39.5 centimeters), which is preserved in the Biblioteca Nazionale Centrale di Roma (Fondo Gesuitico, number 763), is attached to a handwritten report dated 1635. The anonymous author of the report, who possibly also made the drawing, was an eyewitness to the eruption from 19 December 1634 to at least 17 January 1635. The eyewitness saw the eruption from Catania and other villages around the volcano. He declared in the detailed report that he painstakingly observed the sites and that the topographic information he provided is correct, since he had been helped by a local guide who was an expert on the volcano. According to the report, handwritten in Italian in early January 1635, the eyewitness went on a guided excursion close to the active crater.

Along with the report, there is a drawing with notations in Latin. In the graphically elementary watercolor drawing, lava is red, the ground is ochre, and the then perennial "snow zone"—which is now sporadic—is white. Seven locations are localized with a black dot, but only four toponyms are reported.

The report only describes four of the seven lava flows portrayed in the drawing, so the map and the report complement each other with different information. The report notes that only one flow emerged from the crater and that this flow reached as far as the Piano delle Rosselle (Roselle Plain). This is a large concave area where lava accumulated for several days because the path to the south and to Catania was blocked by a hill called Salto del Cane
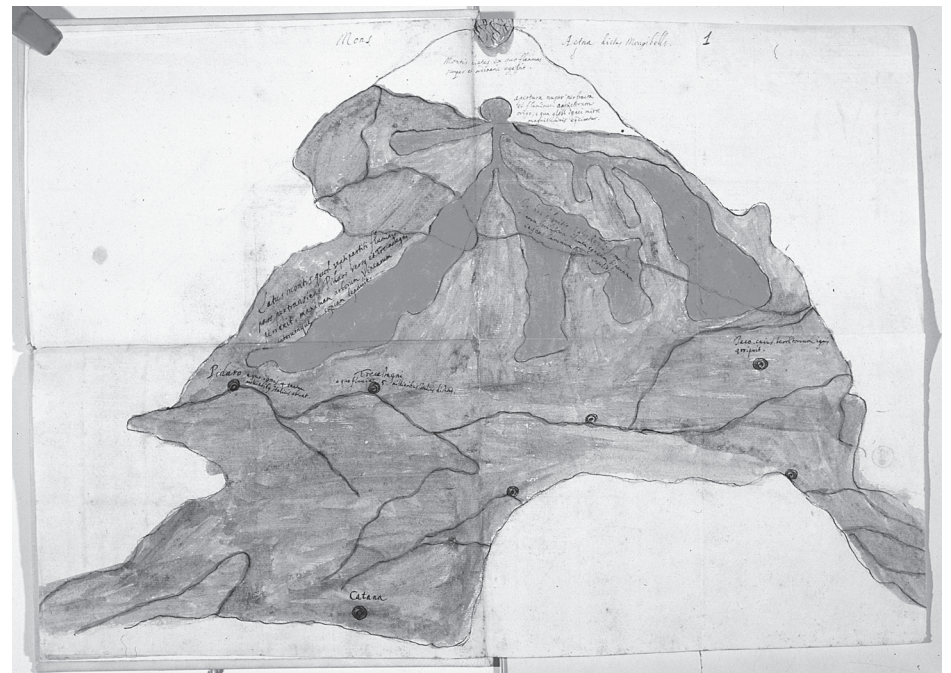

Fig. 1. Map 1 is a watercolor sketch showing Mount Etna erupting, 1634. Red indicates lava; ochre indicates ground; white indicates the so-called zone of the perennial snows, which no longer exists. Courtesy Biblioteca Nazionale Centrale di Roma. Original color image appears at the back of this volume.

(a) Horizontal fault slip vectors are measured from linear least squares adjustment on each side of the fault and on each N-S and E-W component of profiles running perpendicularly to the fault. Profiles are stacked over a width of 2 km. This produces the vector plot of the displacement at fault, showing right-lateral strike-slip motion. Ellipses represent the 95% confidence interval.
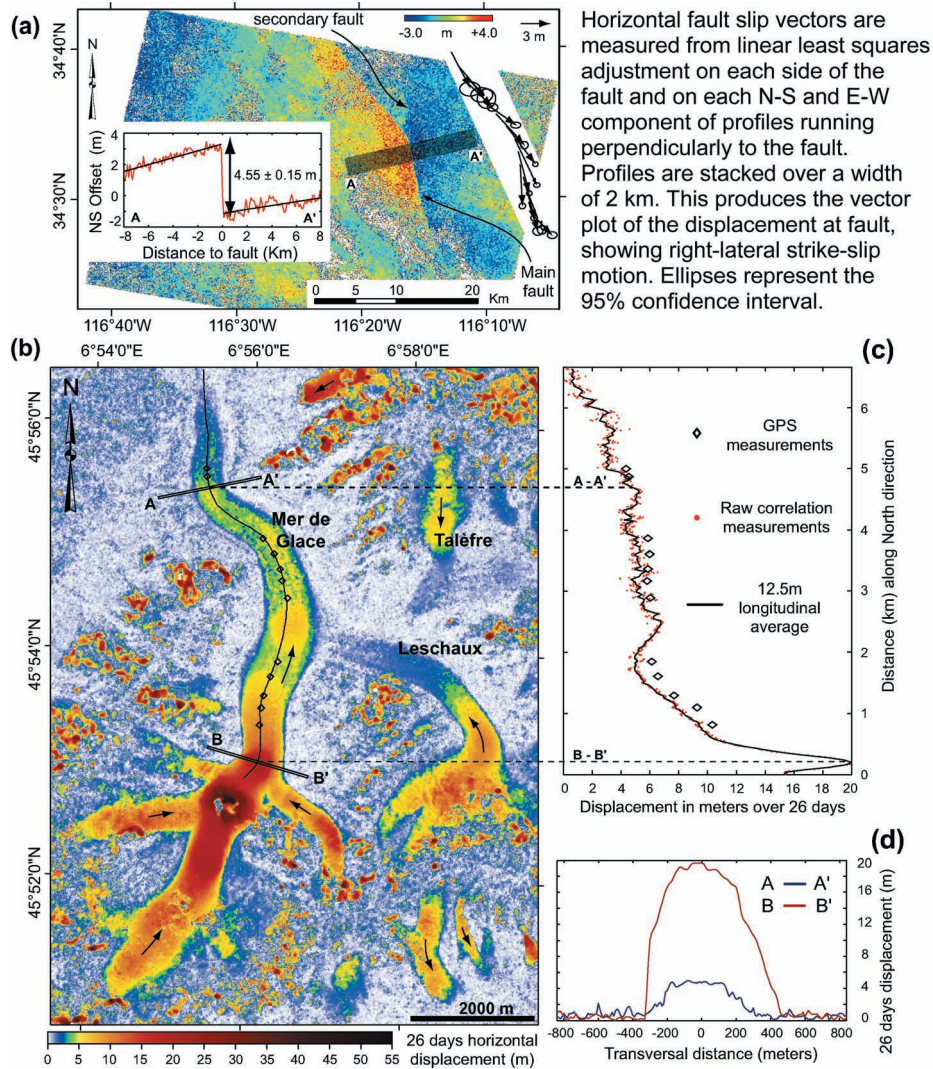
Fig. 1. (a) North/south component (northward positive) of the coseismic displacement field due to the 1999 Hector Mine earthquake in California. The pre-earthquake image (10-meter SPOT 4 acquisition from 17 August 1998) and the post-earthquake image (15-meter ASTER acquisition from 10 May 2000) were orthorectified and coregistered on a 10-meter-resolution grid, and offsets were measured from subpixel correlation between sliding windows. No measurement is assigned to white points where the correlation is too weak. The main fault rupture is a linear discontinuity in the data. The standard deviation on individual measurements is around 1.3 meters. (b) Amplitude of the horizontal displacement over the Mer de Glace area from 23 August 2003 to 18 September 2003, obtained from two panchromatic 2.5-meter-resolution SPOT 5 images. Arrows indicate the flow direction. Displacements below the images' resolution appear in blue. Displacements as high as 55 meters (about 800 meters per year) are recorded over this 26-day period. (c) Displacements along a central flow line of the Mer de Glace measured from SPOT 5 images and from campaign GPS. The time period covered by the GPS (12 August 2003 to 3 September 2003) starts slightly earlier in the summer and includes the August 2003 European heat wave, which explains the faster velocities observed over this period [Berthier et al., 2005]. (d) Displacement along transverse profiles AA' and BB'.

Fig. 2. (a) Orthorectified SPOT image of the La Valette landslide (Ubaye Valley, French Alps). The red diamonds show the geodetic benchmarks for field survey. (b) Absolute horizontal displacement and displacement vectors as imaged from the correlation of two 2.5-meter SPOT 5 images acquired on 19 September 2003 and 22 August 2004. The maximum displacement is 9 meters. Longitudinal and transversal profiles, along AA' and BB', respectively, show the raw data (red dots) and the average over a 15-meter-wide swath (gray line). The black diamonds indicate the geodetic benchmarks. The displacement field revealed from the correlation would not have been noticed in the geodetic measurements.

Page 2

Fig. 1. Map 1 is a watercolor sketch showing Mount Etna erupting, 1634. Red indicates lava; ochre indicates ground; white indicates the so-called zone of the perennial snows, which no longer exists. Courtesy Biblioteca Nazionale Centrale di Roma.